NANO LETTERS

LETTER

pubs.acs.org/NanoLett

Tuning Structure and Properties of Graded Triblock Terpolymer-Based Mesoporous and Hybrid Films

William A. Phillip,[*,†,∥,⊥] Rachel Mika Dorin,[‡,∥] Jörg Werner,[‡,#] Eric M. V. Hoek,[§] Ulrich Wiesner,[‡] and Menachem Elimelech[†]

[†]Department of Chemical and Environmental Engineering, P.O. Box 208286, Yale University, New Haven, Connecticut 06520-8286, United States

[‡]Department of Materials Science and Engineering, 214 Bard Hall, Cornell University, Ithaca, New York 14853-1501, United States

[§]Department of Civil and Environmental Engineering, P.O. Box 952593, University of California, Los Angeles, Los Angeles, California 90095-1593, United States

Supporting Information

ABSTRACT: Despite considerable efforts toward fabricating ordered, water-permeable, mesoporous films from block copolymers, fine control over pore dimensions, structural characteristics, and mechanical behavior of graded structures remains a major challenge. To this end, we describe the fabrication and performance characteristics of graded mesoporous and hybrid films derived from the newly synthesized triblock terpolymer, poly(isoprene-*b*-styrene-*b*-4-vinylpyridine). A unique morphology, unachievable in diblock copolymer systems, with enhanced mechanical integrity is evidenced. The film structure comprises a thin selective layer containing vertically aligned and nearly monodisperse mesopores at a density of more than 10^{14} per m^2 above a graded macroporous layer. Hybridization via homopolymer blending enables tuning of pore size within the range of 16 to 30 nm. Solvent flow and solute separation experiments demonstrate that the terpolymer films have permeabilities comparable to commercial membranes, are stimuli-responsive, and contain pores with a nearly monodisperse diameter. These results suggest that moving to multiblock polymers and their hybrids may open new paths to produce high-performance graded membranes for filtration, separations, nanofluidics, catalysis, and drug delivery.

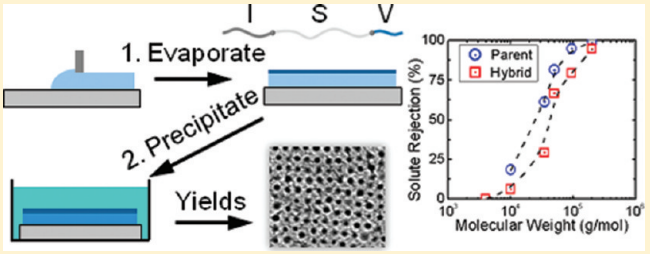

KEYWORDS: Triblock terpolymer, self-assembly, mesoporous, membranes, polyisoprene-*b*-polystyrene-*b*-poly-4-vinyl pyridine, filtration

Understanding and controlling the transport of chemical species at the nanoscale will enable the design of novel devices and systems capable of addressing several of the issues facing chemical separations (e.g., water purification[1] and bioseparations[2]), drug delivery, and molecular sensing.[3] Many of these technologies will rely on a membrane or thin film with robust mechanical properties and well-controlled pore dimensions and chemistries. In order to advance the understanding and implementation of technologies that exploit transport phenomena at the nanoscale, it is essential to make progress toward fabrication and characterization of next generation, high-performance mesoporous materials.

One promising route to major improvements in this research area is the formation of mesoporous and hybrid films through block copolymer self-assembly.[4,5] Block copolymers, an intriguing class of macromolecules known to microphase separate into periodic, ordered structures with length scales typically ranging from 5 to 50 nm, offer a functional approach for designing a versatile assortment of mesoscale hybrid materials, such as patterned media[6,7] and devices, including batteries,[8,9] solar cells,[10,11] and fuel cells.[12] In addition to applications in drug delivery and nanofluidics, copolymer-derived mesoporous films are strong candidates as highly selective separation membranes.

Membranes based on diblock copolymer and triblock terpolymer self-assembly have been generated through bulk casting, but these nongraded materials suffer from low permeabilities due to relatively thick selective layers, and hybrids were not investigated.[13−16] Mesoporous thin films from diblock copolymers have been fabricated by spin coating onto solid substrates; however, this method requires long annealing times and the tedious transfer of a fragile thin film from the primary substrate to a secondary support membrane.[17−20] A third approach combines the self-assembly of diblock copolymers with nonsolvent-induced phase separation; however, a thorough performance evaluation of the resulting membranes has not yet been attempted, and the use of glassy diblock copolymers in this system reduces the opportunity for chemical and mechanical tunability.[21,22]

Received: April 22, 2011
Revised: May 21, 2011
Published: June 07, 2011

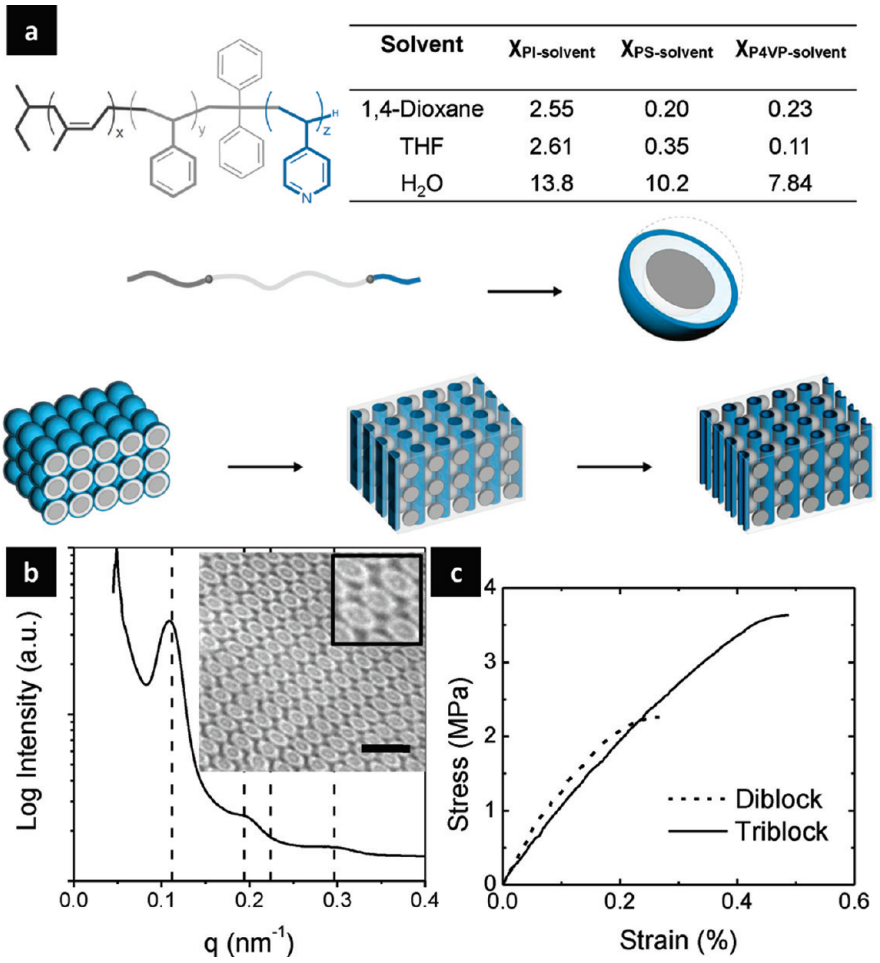

Figure 1. Mesoporous films are cast from a poly(isoprene-*b*-styrene-*b*-4-vinyl pyridine) triblock terpolymer. (a) The structure of the ISV terpolymer, table indicating the polymer−solvent interaction parameters as calculated from solubility parameters and proposed formation mechanism of the separation layer. (b) SAXS trace of the bulk ISV material. Dashed lines correspond to peak positions $(q/q^*)^2 = 1, 3, 4$, and 7, expected for a hexagonal lattice. Inset: TEM image of the terpolymer film selectively stained with OsO_4. The scale bar is 100 nm. The higher magnification inset displays the interconnected white polystyrene regions and is 100 nm on each side. The darkest regions correspond to the PI, the gray regions to the P4VP, and the white regions to the PS domains. (c) Stress−strain curves of the bulk triblock terpolymer and diblock copolymer films.

Here we describe the facile and scalable fabrication of novel, graded, ABC-type triblock terpolymer-derived mesoporous films, and elucidate the benefits of utilizing a multiblock polymer system. The structural and performance characteristics of the mesoporous films, including both stimuli responsive permeation and separation, are shown. Pore size tunability through simple hybridization via polymer blending and the subsequent effect on separation performance is reported. Both parent terpolymer and hybrid films contain more than 10^{14} pores/m^2, have permeabilities comparable to commercial ultrafiltration membranes, and solute separations consistent with films containing monodisperse mesopores.

A novel triblock terpolymer, poly(isoprene-*b*-styrene-*b*-4-vinylpyridine) (ISV), was synthesized by anionic polymerization as the starting material for the formation of the graded mesoporous films described herein. A detailed description of the synthetic procedure can be found in the Supporting Information. Figure 1a shows the chemical structure of the terpolymer together with a table of the polymer−solvent interaction parameters, χ_{1-2}, for the different solvents used here, as calculated from solubility parameters.[23] The material used in this study, referred to as ISV-77, had a total molar mass of 76.6 kg/mol, a polydispersity of 1.16, and volume fractions of 0.29, 0.56, and 0.15 for the polyisoprene (PI), polystyrene (PS), and poly-4-vinylpyridine (P4VP) domains, respectively. Figure 1b shows both a small-angle X-ray scattering (SAXS) trace and a transmission electron microscopy (TEM) micrograph of a bulk ISV-77 film cast from chloroform, both of which are consistent with a hexagonally close packed cylinder morphology, where P4VP forms the cylinder cores.

In order to get an impression of the mechanical response of this material relative to a diblock copolymer of similar molecular characteristics, Figure 1c compares representative stress strain curves for bulk ISV-77 and a bulk poly(styrene-*b*-4-vinylpyridine) (SV) sample with hexagonal P4VP cylinder morphology (data not shown). The SV diblock molar mass was 56 kg/mol with polydispersity of 1.19, and volume fractions of 0.71 and 0.29 for PS and P4VP, respectively. The area under the ISV-77 curve, representing the toughness of the material, is 9.0 GJ/m^3, almost triple that of the 3.20 GJ/m^3 toughness of the glassy SV, which can be attributed to the addition of the rubbery, low T_g polyisoprene domain.[24] The results of these tensile tests suggest that the ISV polystyrene

dx.doi.org/10.1021/nl2013554 |*Nano Lett.* 2011, 11, 2892–2900

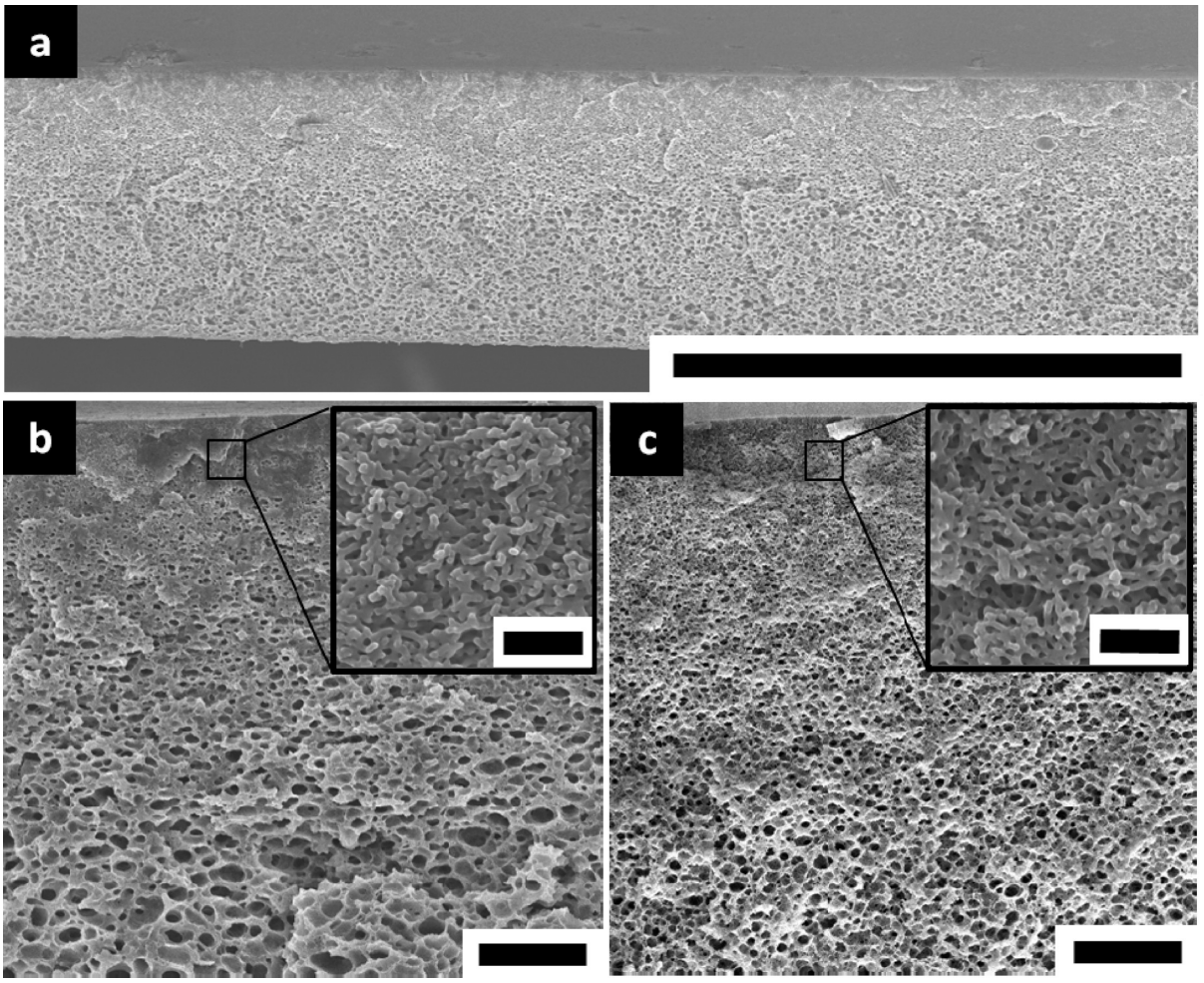

Figure 2. The nonsolvent induced phase separation process forms a spongelike, graded structure in the membranes. (a) Low-magnification SEM micrograph of the cross-section of an ISV-77 film. Scale bar is 100 μm. (b) Cross-sectional SEM of the as cast parent terpolymer film shows that the bottom of the film is macroporous and becomes denser as proximity to the top selective layer increases. Inset: higher-magnification image of the phase inverted structure just below the separation layer shows that the region contains macropores. (c) Cross-sectional SEM of the hybrid membrane displaying a similar graded structure. Inset: higher-magnification image of the phase inverted structure just below the separation layer displays increased porosity compared to the parent structure. The scale bars for panels b and c are 5 μm and 500 nm in the main images and insets, respectively.

domains are interconnected, which is evidenced by a more careful look at the morphology of this cast material (inset in Figure 1b). This simple bulk comparison demonstrates the potential for tuning the mechanical response of mesostructured materials by moving from diblock to multiblock systems.[25] Other advantages include the expanded phase space over which triblock terpolymers and other multiblock systems exhibit bicontinuous morphologies, which have been shown to exhibit enhanced mechanical properties due to the continuity of multiple domains,[26,27] as well as additional control over chemical functionality.[4]

The graded, mesoporous terpolymer films are formed using a combination of controlled solvent evaporation and nonsolvent-induced phase separation[28] (NIPS). The solvent evaporation directs the self-assembly of the terpolymer to template the structure of the mesoporous selective layer, and the subsequent NIPS process creates the underlying macroporous support structure. A vast parameter range was screened to find appropriate film formation conditions. The protocol for casting a film begins by dissolving the ISV in an appropriate solvent. This solvent must fulfill two requirements; it must result in the desired orientation of self-assembled morphology at the top surface of the film upon evaporation,[29] and it must be miscible with the nonsolvent for the NIPS process. From the large library of possible solvents, we found that a mixture of 1,4-dioxane/tetrahydrofuran (70/30 by weight) fulfilled both these requirements.

A 12 wt % polymer solution was drawn into a film on a glass substrate using a doctor's blade set at a gate height of 225 μm. After the film was cast, the solvent was allowed to evaporate for a predetermined period of time, during which the concentration of polymer at the air/film interface increased. The film was subsequently plunged into a nonsolvent (water) bath, causing the precipitation of the underlying polymer into an asymmetric macroporous structure. The selection of polymer concentration, substrate, and gate height all affect the ultimate macro- and mesostructure of the resulting film and were carefully optimized. For example, low polymer concentrations (<10 wt %) resulted in low polymer connectivity upon plunging in the nonsolvent, while a hydrophobic Teflon substrate caused the film to dewet. A large gate height (>400 μm) yielded cracks in the film due to instabilities at the free surface.

Scanning electron microscopy (SEM) micrographs of the cross-section of ISV-77 films are shown at different magnifications

dx.doi.org/10.1021/nl2013554 |*Nano Lett.* 2011, 11, 2892–2900

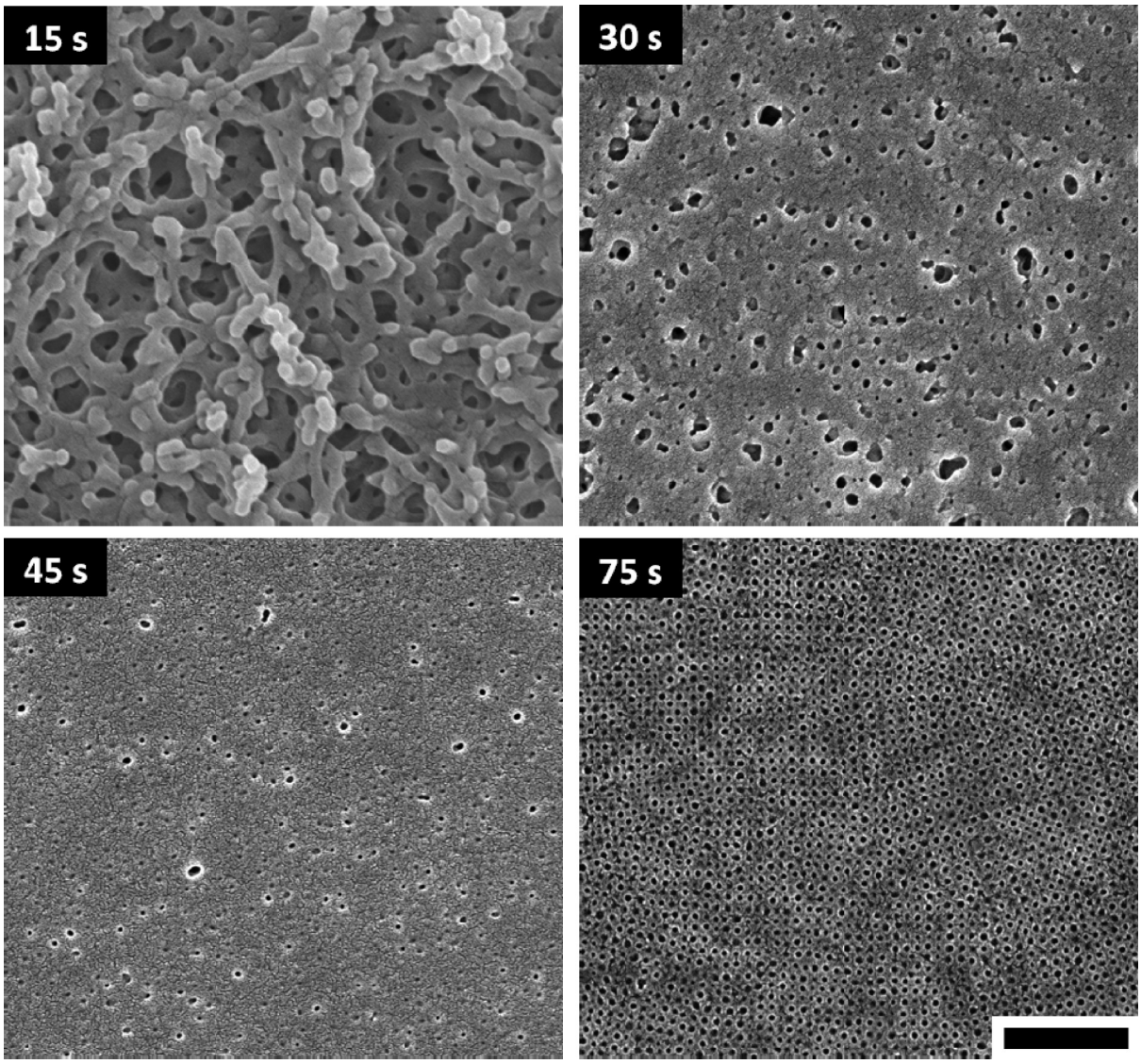

Figure 3. SEM micrographs show that the structure of the thin film surface changes with the length of the solvent evaporation period. Poly(isoprene-*b*-styrene-*b*-4 vinyl pyridine) thin films were cast from a 12 wt % solution of polymer in solvent. The solvent used was a 70/30 mixture (w/w) of dioxane and tetrahydrofuran (THF). After drawing down a thin film of polymer solution, the solvent was allowed to evaporate for a predetermined period of time before plunging the film into a nonsolvent (water) bath to initiate phase separation. For short evaporation times (15 and 30 s), a dense layer does not form, producing macroporous films. At intermediate evaporation times (45 s), a dense layer forms, but the self-assembled terpolymer structure has just begun to nucleate resulting in few pores. Given sufficient time (75 s), the self-assembled structure nucleates and grows into the film producing a thin film with a high density of nanopores. All images are shown at the same resolution and the scale bar is 500 nm.

in Figure 2a,b and display the asymmetric structure that results from the protocol described above. The film is densest at the top surface where the polymer concentration was highest prior to beginning the NIPS process. The substructure pores increase in size and the film becomes more open toward the bottom surface. Sheets of 40 μm thick ISV-77 mesoporous films as large as 300 cm^2 were fabricated in the lab for permeability and solute separation testing. This fabrication method has the important benefit of industrial scalability.[30]

The length of the solvent evaporation step is another process variable that significantly affects the final structure of the film. Specifically, the solvent evaporation step is critical to directing the self-assembly of the terpolymer. Solvent evaporation into the open atmosphere created fast evaporation conditions, which can be used to orient the cylindrical domains perpendicular to the thin dimension of the film.[16,29,31] Figure 3 shows SEM micrographs of the top surface of films cast under identical conditions but with solvent evaporation times of 15, 30, 45, and 75 s. These micrographs elucidate the film structure dependence on the length of the evaporation step. For short evaporation times (i.e., 15 and 30 s), the local concentration of polymer was not high enough to form a dense skin layer. Thus, when the film was plunged into the water bath, a macroporous structure resulted even at the surface. Open network structures formed when an evaporation time of 15 s was used, while at 30 s dense regions were observed with pores 50−200 nm in diameter randomly distributed across the surface. The film cast using a 45 s evaporation period had a dense skin layer, but only a few nanopores began to nucleate at the surface. Allowing the solvent to evaporate for 75 s produced the desired nanostructure, which is a

dx.doi.org/10.1021/nl2013554 |*Nano Lett.* 2011, 11, 2892–2900

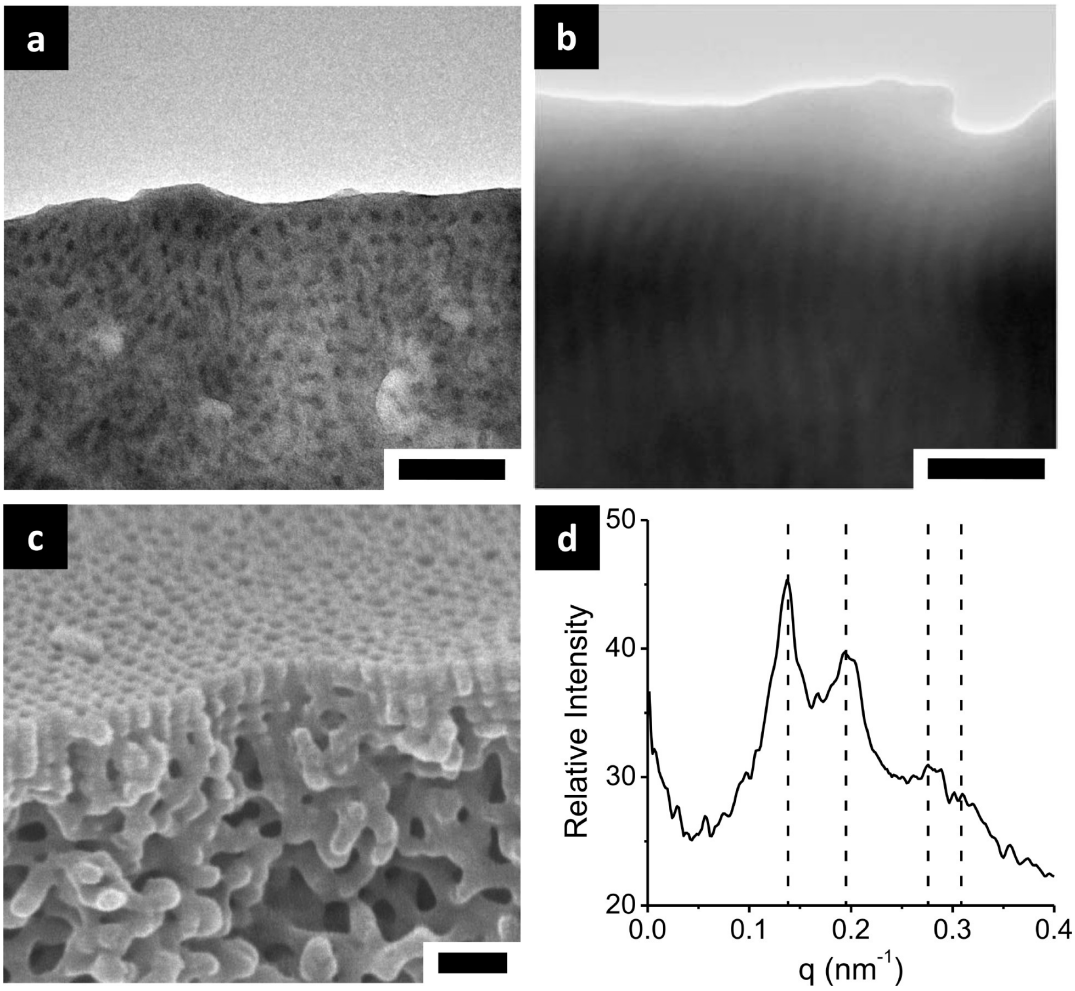

Figure 4. The self-assembled structure of the selective layer is a kinetically trapped, nonequilibrium structure. (a) Cubically packed polyisoprene spheres are identified by TEM where the PI domains were stained with OsO_4. (b) A TEM micrograph of the selective layer with P4VP domains stained with I_2 demonstrates P4VP channels run through the selective layer. (c) A cross sectional SEM micrograph shows open pores spanning the selective layer thickness, consistent with the I_2 stained TEM micrograph. All scale bars are equal to 100 nm. (d) Radially integrated FFT of an SEM image of the top surface of the film. Dashed lines correspond to $(q/q^*)^2 = 1, 2, 4$, and 5, consistent with pores packed in a square lattice and yielding a *d*-spacing of 44 nm.

selective skin layer containing a high density of nanopores ~20 nm in diameter. The narrow pore size distribution suggests that their structure is a result of the triblock terpolymer self-assembly.

Cross sections of the self-assembled surface structure are readily visualized by transmission and scanning electron microscopy (Figure 4a–c). Figure 4a,b shows TEM micrographs of films selectively stained with OsO_4 (PI selective stain) and I_2 (P4VP selective stain), respectively. In Figure 4a, the circular dark regions, which appear cubically packed at the top, correspond to the stained PI of the terpolymer. This intriguing structure is reminiscent of high impact polystyrene (HIPS) in which rubbery inclusions act to dissipate stress from the glassy PS surrounding it. Indeed, this affords the film increased resistance against fracture,[32] which makes handling of these membranes much easier than membranes derived from SV diblock copolymers (Figure 1c). In Figure 4b, the P4VP domains appear as the dark lines running vertically through the film. These domains are consistent with the mesopores running from the top surface into the underlying macroporous support, as corroborated by the SEM micrograph in Figure 4c. These channels act as highly uniform mesopores through which gases or liquids can be transported and potentially separated. Interestingly, closer examination of the mesopores on the top surface of the terpolymer film reveals that their packing is in a square lattice rather than in a hexagonal array, as seen in the equilibrium bulk morphology. Figure 4d shows a radially integrated FFT of an SEM micrograph of the top surface where indices consistent with a square packed lattice are marked. From this data, a pore *d*-spacing of 44 nm and an areal pore density of 5.2×10^{14} pores/m^2 can be calculated.

The results above demonstrate our ability to fabricate large areas of mesoporous films containing a high density of nearly monodisperse pores. The unique kinetically trapped structure of the films can be further studied by measuring transport properties, such as the permeability to liquids or gases and the ability to selectively separate dissolved solutes. These experiments not only provide more insight into the nanostructure of the film but are also critical to examining the utility of the films in membrane filtration, drug delivery, and sensing applications.

Results of flow experiments conducted with acetate buffer solutions between pH 4 and 6 are shown in Figure 5a; the hydraulic

dx.doi.org/10.1021/nl2013554 |*Nano Lett.* 2011, 11, 2892–2900

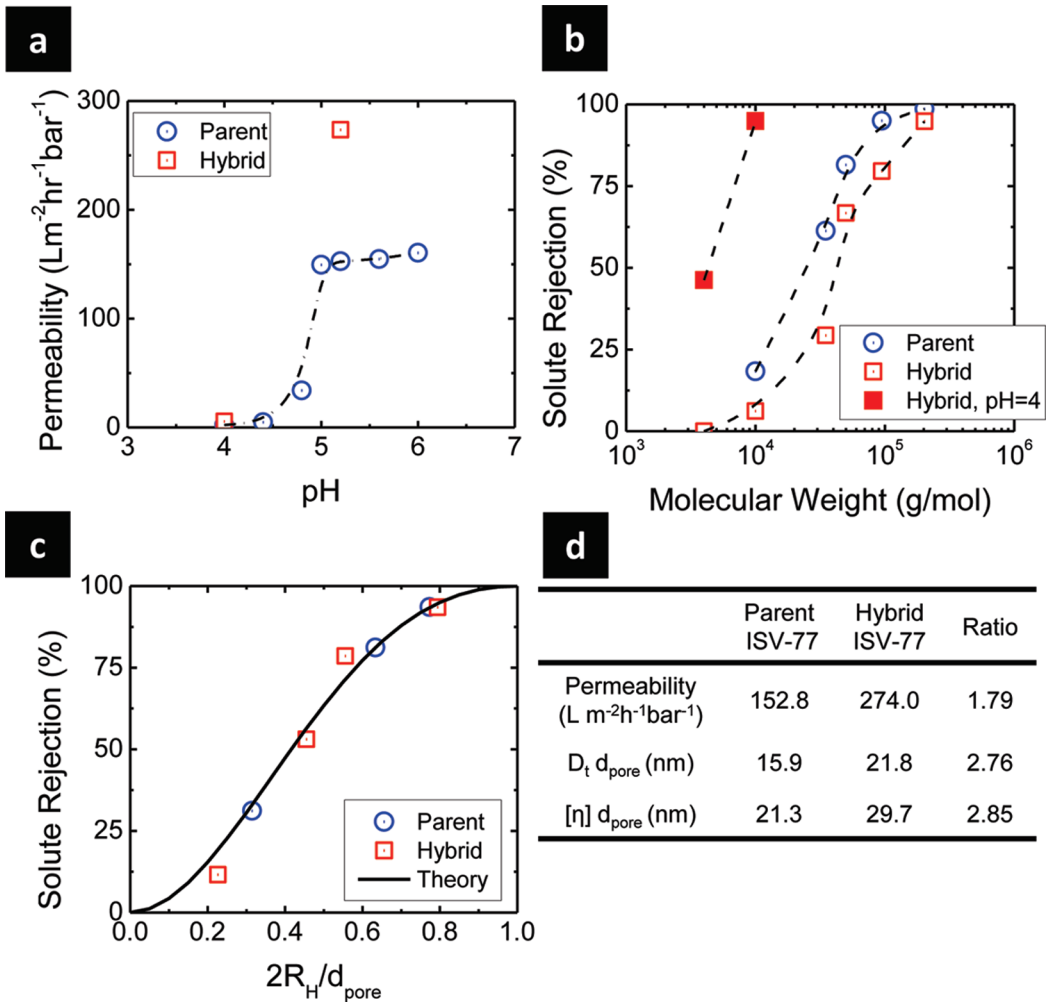

	Parent ISV-77	Hybrid ISV-77	Ratio
Permeability (L m^{-2}h^{-1}bar^{-1})	152.8	274.0	1.79
D_t d_{pore} (nm)	15.9	21.8	2.76
[η] d_{pore} (nm)	21.3	29.7	2.85

Figure 5. Transport behavior of the mesoporous parent and hybrid films. (a) Solution permeation was measured on a 4.1 cm^2 area of membrane at a pressure drop of 0.345 bar using buffer solutions of sodium acetate and acetic acid at varying pH. For membranes cast without swelling agents the hydraulic permeability ranges from 2.2 to 160 L m^{-2}h^{-1}bar^{-1} at pH = 4 to pH = 6, respectively. Membranes cast with swelling agents had a hydraulic permeability of 5.4 L m^{-2} h^{-1} bar^{-1} at pH = 4 and 274 L m^{-2} h^{-1} bar^{-1} at pH = 5.2. (b) The nanoporous thin films reject dissolved solutes. Polyethylene oxide (PEO) molecules with molar masses of 4, 10, 35, 50, 95, and 203 kg/mol were dissolved at a concentration of 1 g/L. Parent and hybrid films were challenged with PEO in DI water, and the hybrid film was also challenged with PEO in acetate buffer at pH 4. Feed and permeate samples were collected and the PEO concentrations determined using total organic carbon analysis. (c) The pore size of the ISV-77 and hybrid ISV-77 films are estimated by fitting the experimental rejection data with a theory for the hindered transport of solutes in cylindrical pores. The data point at $2R_H/d_{pore} \approx 0.8$ for the parent ISV-77 film is for the 50 kg/mol PEO molecule while for the hybrid ISV-77 film it is for the 95 kg/mol PEO sample. (d) Table of the hydraulic permeabilites and calculated pore diameters from diffusion and intrinsic viscosity data. For the hydraulic permeabilities, the ratio column is the quotient of the two values, while for the pore diameter this column represents the ratio of εd^2_{pore}.

permeability of the films was a strong function of pH. At pH 5 and higher, there was a small increase in permeability with increasing pH. Below a pH of 5, the permeability decreased rapidly, reaching a value of 2.2 L m^{-2} hr^{-1} bar^{-1} at pH 4, nearly 80 times lower than the permeability at pH 6 of 160 L m^{-2} hr^{-1} bar^{-1}.

The stimuli responsive permeability provides evidence that the mesopores are coated with a P4VP brush,[33,34] consistent with the micrographs in Figures 3 and 4. P4VP has a pK_a of 4.6, which is near the pH where our films become pH responsive. At pH values below the pK_a, the degree of protonation of the P4VP is higher, making it more soluble in the aqueous buffer solutions. The better solvated P4VP extends toward the center of the pore, slowing the flow of the aqueous solution. Conversely, deprotonated P4VP is not well solvated by the solutions and retracts against the pore walls to open the pores to flow. Similar results were obtained using a 50/50 (w/w) solution of ethanol/deionized water (DI water). In the presence of ethanol, which is a good solvent for P4VP, the permeability decreases to values similar to that at pH 4. These results suggest that it is the solvent quality for P4VP that results in the stimuli responsive nature of the films.

Solute separation (rejection) tests are a similarly valuable tool for exploring the structure of the mesoporous films, and critical to confirming an absence of defects. Single solute PEO samples dissolved in DI water and ranging in molar mass from 4 to 203 kg/mol were used to challenge the films. Observed percent rejections were calculated by comparing the PEO concentration in the permeate and feed solutions. Results from these experiments are shown as open circles in Figure 5b. As the PEO molar mass increases, the percent rejection also increases. For example, a 10 kg/mol sample was only slightly rejected

dx.doi.org/10.1021/nl2013554 |Nano Lett. 2011, 11, 2892–2900

(~18% rejection) while a 95 kg/mol sample was almost completely rejected (~95% rejection).

The solute rejection data can be used to estimate the pore size of the film. However, it is important to ensure the calculation of an intrinsic film property, and not an experimental artifact. Therefore, the observed solute rejections were converted to actual (or intrinsic) rejections to account for the local increase in the concentration of rejected solutes at the film interface due to concentration polarization.[35] The mass transfer coefficient necessary for this calculation was determined using the correlation given by Zeman and Zydney.[36] For all rejection experiments, the ratio of the volumetric flux to the mass transfer coefficient was between 0.7 and 1.6, indicating that the system was not highly polarized.

Figure 5c shows the pore diameter of the films as calculated by comparing the actual rejection to a theory for the hindered transport of solutes in cylindrical pores. Because convection dominates transport through the mesopores, the theory of Zeman and Wales was used[37]

$$R = 1 - [(1-\lambda)^2[2-(1-\lambda)^2]\exp(-0.7146\lambda^2)] \quad (1)$$

This simplified expression for the solute rejection, R, which gives results within 2% of more complicated expressions,[36] is a function of λ, defined as the ratio of the solute size to the pore size. The hydrodynamic radius of PEO, R_H, was taken as the characteristic solute size. R_H can be calculated from either tracer diffusion[38] or intrinsic viscosity[39] data sets, both of which are available in the literature. Using d_{pore} as an adjustable parameter, the residual squared was minimized. This method gave d_{pore} values of 15.9 and 21.3 nm when tracer diffusion and intrinsic viscosity were used to determine $2R_H$, respectively, and are in good agreement with the SEM micrograph in Figure 3.

The ability to finely tune structural parameters by hybridization with other materials, thus tailoring, for example, the transport properties of the terpolymer films, is another exciting feature of these materials. For example, hybrid films fabricated by blending of a homopolymer that preferentially partitions into one domain of the block terpolymer can be utilized. These terpolymer/homopolymer blends selectively increase the size of the specified terpolymer domain, as demonstrated by the results shown in Figure 5. Here, P4VP homopolymer with molar mass 5.1 kg/mol and polydispersity 1.06 was blended with the terpolymer in the casting solution to swell the effective volume fraction of P4VP from 0.15 to 0.22. Transport tests were used to confirm this observation. The open square data in Figure 5a shows that these hybrid films remain stimuli responsive. At pH = 4, the permeability is equal to 5.4 L m^{-2} h^{-1} bar^{-1}, which is about 50 times lower than the permeability at pH = 5.2 of 274 L m^{-2} h^{-1} bar^{-1}. These permeabilities measured for the hybrid ISV-77 films are higher than those of the neat ISV-77 films at the same pH, consistent with an increased pore size. Additionally, visual comparison of the pores in the top surface of parent ISV-77 films against homopolymer blended ISV-77 films, shown in Supporting Information Figure S1, confirms that the homopolymer increases the pore diameter.

Figure 5b shows the results of solute rejection tests conducted with the hybrid membranes (open square symbols). These experiments were run at a lower pressure drop to maintain similar hydrodynamic conditions to those used when testing the parent membrane. Following the protocol discussed above, an increased pore diameter of 21.8 and 29.7 nm was calculated for the hybrid membrane, depending on whether tracer diffusion or intrinsic viscosity data was used to calculate the R_H of PEO for experiments run in DI water. Figure 5b also shows the results of solute rejection tests conducted with the hybrid membranes in pH 4 acetate buffer (closed square symbols). The increased rejection of PEO solutes suggests that the protonated P4VP chains extend into the pores at pH 4 and indicates that the pH responsive behavior of the material provides an additional mechanism for tuning pore size. Figure 5c shows the fit obtained when intrinsic viscosity data was used to calculate the characteristic size of PEO.

A summary of the hydraulic permeabilities and estimated pore sizes for the parent and hybrid films is given as a table in Figure 5d. Interestingly, the ratio of the hydraulic permeabilities of the hybrid to the parent film is 1.78, while the ratio of the product of the P4VP volume fraction and pore diameters squared is equal to 2.76 and 2.85 for tracer diffusion and intrinsic viscosity, respectively. Given that the hydraulic permeability of a membrane should vary as εd^2_{pore}, where ε is the void fraction of pores,[40] the lack of a corresponding increase in the ratio for the hybrid membranes suggests an inhibition of flow due to the macroporous support structure. While the homopolymer appears to act as a pore-forming agent in the substructure, as seen from a comparison of the insets of Figure 2b,c, we expect that further improvements in the phase inverted structure would enhance the flux gain exhibited by the blended materials.

With the knowledge gained from the materials characterization and transport experiments, it is instructive to return to Figure 1a and consider the physical processes occurring as the kinetically trapped mesostructure of the selective layer develops. When dissolved in the casting solution, the ISV self-assembles into micelles with PI cores and an outer P4VP corona, which minimizes the unfavorable enthalpic interactions between the casting solvents and the PI chains (see table in Figure 1). We speculate that as the solvent evaporates from the film/air interface, and the local concentration of polymer increases, the terpolymer micelles begin to pack cubically. With further solvent evaporation, the terpolymer eventually feels a driving force to transition to the equilibrium hexagonal cylinder morphology. It has been proposed that the solvent concentration gradient when the micelles begin to transition to a cylinder morphology is responsible for orienting the cylinders perpendicular to the thin dimension of the film.[29] Upon plunging the film into the nonsolvent, the solvent and nonsolvent begin to exchange, causing the ISV to precipitate, trapping the final structure of the selective layer. We hypothesize that the exchange of solvent and nonsolvent also results in the creation of free volume with the P4VP cylinders; as the solvent-swollen P4VP chains within the cylinders come into contact with the nonsolvent, they collapse against the cylinder walls, forming channels of free volume within the cylinders, which is consistent with the observed stimuli responsive transport properties. The presence of free volume is also supported by the solute rejection curves in Figure 5b, which demonstrate a size exclusion rejection, consistent with open pores.

In summary, the results presented here demonstrate the benefits of moving from diblock copolymers to multiblock polymers and their hybrids for the formation of high-performance graded mesoporous materials. Specifically, the tunable structural characteristics, adjustable mechanical properties, and controllable chemical functionalities of multiblock systems,

provide an exceptional platform for the fabrication of graded mesoporous materials. Because of enhancements possible through terpolymers, detailed empirical studies of transport phenomena at the mesoscale were possible, and we anticipate that this study will expand the viability of such multiblock polymer-derived graded structures to a wide variety of fields.

Methods. The poly(isoprene-*b*-styrene-*b*-4-vinylpyridine) triblock terpolymer used in this study was synthesized using a sequential anionic polymerization technique. A detailed description of the synthesis can be found in the Supporting Information. The molecular weight of the terpolymer was determined using gel permeation chromatography, which was performed using THF as a solvent on a Waters 510 GPC instrument equipped with a Waters 2410 differential refractive index (RI) detector. The volume fraction of each block was calculated using the ^{1}H solution nuclear magnetic resonance (^{1}H NMR) spectra obtained on a Varian INOVA 400 MHz spectrometer using $CDCl_3$ (δ = 7.27 ppm) signal as an internal standard.

Large sheets of mesoporous films were cast using the protocol described in the text. Circular samples 2.5 cm in diameter for solvent flow and solute rejection tests were punched out of larger sheets using a hole punch.

Solvent flow experiments were conducted in a stirred cell (Amicon 8010, Millipore Co.). Pressure to drive flow was applied using N_2 gas and was monitored using a digital pressure gauge. DI water was obtained from a Milli-Q ultrapure water purification system. Acetate buffer solutions were prepared by mixing 0.1 M acetic acid and 0.1 M sodium acetate aqueous solutions in the proper proportions. The flow rate was determined by measuring the permeate mass every 5 min. No prewetting step was required for the solvent flow experiments.

Solute rejection tests were performed using single solute PEO solutions at a concentration of 1 g/L in DI water. The experimental procedure followed was similar to that described in the literature.[16] PEO concentration in the feed and permeate was determined using a Shimadzu total organic carbon analyzer. For all experiments, the solution was stirred at a rate of 800 rpm. Tests on the ISV-77 films were run at a constant pressure drop of 5 psi while tests on the swollen ISV-77 films were run at a pressure drop of 3 psi to maintain similar hydrodynamic conditions between the two samples.

For TEM, both the bulk polymer film and the membranes were sectioned at 50−70 nm using a Leica Ultracut UCT cryo-ultramicrotome at −60 °C. Microtomed samples were selectively stained with either OsO_4 (g) for 30 min or with I_2 (g) for 2 h. Bright-field TEM (BF-TEM) images were obtained using a FEI Technai F12 Spirit electron microscope equipped with a SIS Megaview III CCD camera, operated at an acceleration voltage of 120 kV.

SEM micrographs were acquired using a Hitachi ultrahigh resolution analytical field emission scanning electron microscope (FE-SEM) SU-70. Samples were coated with gold−platinum for 30 s prior to imaging using an Emitech SC7620 sputtering machine.

SAXS measurements on the bulk terpolymer were performed at the Cornell High Energy Synchrotron Source (CHESS). The sample to detector distance was approximately 3.3 m. The X-ray wavelength was 1.305 Å, and the scattering vector, $\mathbf{q}$, is defined as $\mathbf{q} = (4\pi/\lambda)\sin\theta$ where θ is half of the scattering vector.

Mechanical tests were performed using a TA Instruments DMAQ800 instrument outfitted with film tension clamps. The films were fixed in the tension clamps with a torque of 0.6 in lb. and preloaded with a force of 0.01 N. Stress−strain curves were obtained using a ramp force of 0.50 N/min.

■ ASSOCIATED CONTENT

Supporting Information. Additional information provided. This material is available free of charge via the Internet at http://pubs.acs.org.

■ AUTHOR INFORMATION

Corresponding Author

*E-mail: wphillip@nd.edu.

Present Addresses

[⊥]Department of Chemical and Biomolecular Engineering, 182 Fitzpatrick Hall, University of Notre Dame, Notre Dame, IN, 46556-5637, United States.

[#]Johannes-Gutenberg University, Institute for Inorganic Chemistry, Duesbergweg 10-14, 55099 Mainz, Germany.

Author Contributions

[‖]These authors contributed equally to this work.

■ ACKNOWLEDGMENT

This publication is based on work supported by Award No. KUS-C1-018-02, made by King Abdullah University of Science and Technology (KAUST). R.M.D. acknowledges support from the NSF Graduate Research Fellowship Program (GRFP).

■ REFERENCES

(1) Shannon, M. A.; Bohn, P. W.; Elimelech, M.; Georgiadis, J. G.; Marinas, B. J.; Mayes, A. M. Science and technology for water purification in the coming decades. *Nature* **2008**, *452* (7185), 301–310.

(2) van Reis, R.; Zydney, A. Bioprocess membrane technology. *J. Membr. Sci.* **2007**, *297* (1−2), 16–50.

(3) Bohn, P. W. Nanoscale Control and Manipulation of Molecular Transport in Chemical Analysis. *Annu. Rev. Anal. Chem.* **2009**, *2* (1), 279–296.

(4) Jackson, E. A.; Hillmyer, M. A. Nanoporous Membranes Derived from Block Copolymers: From Drug Delivery to Water Filtration. *ACS Nano* **2010**, *4* (7), 3548–3553.

(5) Hillmyer, M., Nanoporous Materials from Block Copolymer Precursors. In *Block Copolymers II*; Abetz, V., Ed.; Springer: Berlin/Heidelberg, 2005; Vol. 190, pp 137−181.

(6) Park, M.; Harrison, C.; Chaikin, P. M.; Register, R. A.; Adamson, D. H. Block copolymer lithography: Periodic arrays of similar to 10(11) holes in 1 square centimeter. *Science* **1997**, *276* (5317), 1401–1404.

(7) Kim, S. O.; Solak, H. H.; Stoykovich, M. P.; Ferrier, N. J.; de Pablo, J. J.; Nealey, P. F. Epitaxial self-assembly of block copolymers on lithographically defined nanopatterned substrates. *Nature* **2003**, *424* (6947), 411–414.

(8) Singh, M.; Odusanya, O.; Wilmes, G. M.; Eitouni, H. B.; Gomez, E. D.; Patel, A. J.; Chen, V. L.; Park, M. J.; Fragouli, P.; Iatrou, H.; Hadjichristidis, N.; Cookson, D.; Balsara, N. P. Effect of molecular weight on the mechanical and electrical properties of block copolymer electrolytes. *Macromolecules* **2007**, *40* (13), 4578–4585.

(9) Panday, A.; Mullin, S.; Gomez, E. D.; Wanakule, N.; Chen, V. L.; Hexemer, A.; Pople, J.; Balsara, N. P. Effect of Molecular Weight and Salt Concentration on Conductivity of Block Copolymer Electrolytes. *Macromolecules* **2009**, *42* (13), 4632–4637.

(10) Crossland, E. J. W.; Kamperman, M.; Nedelcu, M.; Ducati, C.; Wiesner, U.; Smilgies, D. M.; Toombes, G. E. S.; Hillmyer, M. A.; Ludwigs, S.; Steiner, U.; Snaith, H. J.; Bicontinuous Double, A Gyroid Hybrid Solar Cell. *Nano Lett.* **2009**, *9* (8), 2807–2812.

(11) Segalman, R. A.; McCulloch, B.; Kirmayer, S.; Urban, J. J. Block Copolymers for Organic Optoelectronics. *Macromolecules* **2009**, *42* (23), 9205–9216.

(12) Orilall, M. C.; Matsumoto, F.; Zhou, Q.; Sai, H.; Abruna, H. D.; DiSalvo, F. J.; Wiesner, U. One-Pot Synthesis of Platinum-Based Nanoparticles Incorporated into Mesoporous Niobium Oxide-Carbon Composites for Fuel Cell Electrodes. *J. Am. Chem. Soc.* **2009**, *131* (26), 9389–9395.

(13) Cooney, D. L.; Hillmyer, M. A.; Cussler, E. L.; Moggridge, G. D. Diffusion In Nanoporous Materials Made from Block Copolymers. *Crystallogr. Rev.* **2006**, *12* (1), 13–24.

(14) Phillip, W. A.; Rzayev, J.; Hillmyer, M. A.; Cussler, E. L. Gas and water liquid transport through nanoporous block copolymer membranes. *J. Membr. Sci.* **2006**, *286* (1−2), 144–152.

(15) Phillip, W. A.; Amendt, M.; O'Neill, B.; Chen, L.; Hillmyer, M. A.; Cussler, E. L. Diffusion and Flow Across Nanoporous Polydicyclopentadiene-Based Membranes. *ACS Appl. Mater. Interfaces* **2009**, *1* (2), 472–480.

(16) Phillip, W. A.; O'Neill, B.; Rodwogin, M.; Hillmyer, M. A.; Cussler, E. L. Self-Assembled Block Copolymer Thin Films as Water Filtration Membranes. *ACS Appl. Mater. Interfaces* **2010**, *2* (3), 847–853.

(17) Yang, S. Y.; Ryu, I.; Kim, H. Y.; Kim, J. K.; Jang, S. K.; Russell, T. P. Nanoporous membranes with ultrahigh selectivity and flux for the filtration of viruses. *Adv. Mater.* **2006**, *18* (6), 709.

(18) Li, X. F.; Fustin, C. A.; Lefevre, N.; Gohy, J. F.; De Feyter, S.; De Baerdemaeker, J.; Egger, W.; Vankelecom, I. F. J. Ordered nanoporous membranes based on diblock copolymers with high chemical stability and tunable separation properties. *J. Mater. Chem.* **2010**, *20* (21), 4333–4339.

(19) Yang, S. Y.; Park, J.; Yoon, J.; Ree, M.; Jang, S. K.; Kim, J. K. Virus filtration membranes prepared from nanoporous block copolymers with good dimensional stability under high pressures and excellent solvent resistance. *Adv. Funct. Mater.* **2008**, *18* (9), 1371–1377.

(20) Kim, J. K.; Yang, S. Y.; Yang, J. A.; Kim, E. S.; Jeon, G.; Oh, E. J.; Choi, K. Y.; Hahn, S. K. Single-File Diffusion of Protein Drugs through Cylindrical Nanochannels. *ACS Nano* **2010**, *4* (7), 3817–3822.

(21) Peinemann, K. V.; Abetz, V.; Simon, P. F. W. Asymmetric superstructure formed in a block copolymer via phase separation. *Nat. Mater.* **2007**, *6* (12), 992–996.

(22) Nunes, S. P.; Sougrat, R.; Hooghan, B.; Anjum, D. H.; Behzad, A. R.; Zhao, L.; Pradeep, N.; Pinnau, I.; Vainio, U.; Peinemann, K. V. Ultraporous Films with Uniform Nanochannels by Block Copolymer Micelles Assembly. *Macromolecules* **2010**, *43* (19), 8079–8085.

(23) Hansen, C. M. *Hansen Solubility Parameters: A User's Handbook*; CRC Press: Boca Raton, FL, 2000.

(24) Young, R. J.; Lovell, P. A. *Introduction to Polymers*, 2nd ed.; CRC Press: Boca Raton, FL, 1991.

(25) Phatak, A.; Lim, L. S.; Reaves, C. K.; Bates, F. S. Toughness of glassy-semicrystalline multiblock copolymers. *Macromolecules* **2006**, *39* (18), 6221–6228.

(26) Alward, D. B.; Kinning, D. J.; Thomas, E. L.; Fetters, L. J. Effect of Arm Number and Arm Molecular-Weight on the Solid-State Morphology of Poly(Styrene-Isoprene) Star Block Copolymers. *Macromolecules* **1986**, *19* (1), 215–224.

(27) Dair, B. J.; Honeker, C. C.; Alward, D. B.; Avgeropoulos, A.; Hadjichristidis, N.; Fetters, L. J.; Capel, M.; Thomas, E. L. Mechanical properties and deformation behavior of the double gyroid phase in unoriented thermoplastic elastomers. *Macromolecules* **1999**, *32* (24), 8145–8152.

(28) Mulder, M. *Basic Principles of Membrane Technology*, 2nd ed.; Springer: New York, 1996; p 564.

(29) Phillip, W. A.; Hillmyer, M. A.; Cussler, E. L. Cylinder Orientation Mechanism in Block Copolymer Thin Films Upon Solvent Evaporation. *Macromolecules* **2010**, *43* (18), 7763–7770.

(30) Baker, R. W. *Membrane technology and applications*; McGraw-Hill: New York, 2000; pp xii−514.

(31) Kim, G.; Libera, M. Morphological development in solvent-cast polystyrene-polybutadiene-polystyrene (SBS) triblock copolymer thin films. *Macromolecules* **1998**, *31* (8), 2569–2577.

(32) Donald, A. M.; Kramer, E. J. Craze Initiation and Growth in High-Impact Polystyrene. *J. Appl. Polym. Sci.* **1982**, *27* (10), 3729–3741.

(33) Mika, A. M.; Childs, R. F.; Dickson, J. M. Chemical valves based on poly(4-vinylpyridine)-filled microporous membranes. *J. Membr. Sci.* **1999**, *153* (1), 45–56.

(34) Tagliazucchi, M.; Azzaroni, O.; Szleifer, I. Responsive Polymers End-Tethered in Solid-State Nanochannels: When Nanoconfinement Really Matters. *J. Am. Chem. Soc.* **2010**, *132* (35), 12404–12411.

(35) Mehta, A.; Zydney, A. L. Permeability and selectivity analysis for ultrafiltration membranes. *J. Membr. Sci.* **2005**, *249* (1−2), 245–249.

(36) Zeman, L. J.; Zydney, A. L. *Microfiltration and ultrafiltration: principles and applications*; Marcel Dekker: New York, 1996; p xix−618.

(37) Zeman, L.; Wales, M. Polymer Solute Rejection by Ultrafiltration Membranes. In *Synthetic Membranes: Vol. II*, American Chemical Society: Washington, DC, 1981; Vol. 154, pp 411−434.

(38) Faraone, A.; Magazu, S.; Maisano, G.; Migliardo, P.; Tettamanti, E.; Villari, V. The puzzle of poly(ethylene oxide) aggregation in water: Experimental findings. *J. Chem. Phys.* **1999**, *110* (3), 1801–1806.

(39) Meireles, M.; Bessieres, A.; Rogissart, I.; Aimar, P.; Sanchez, V. An Appropriate Molecular-Size Parameter for Porous Membranes Calibration. *J. Membr. Sci.* **1995**, *103* (1−2), 105–115.

(40) Bird, R. B.; Stewart, W. E.; Lightfoot, E. N. *Transport phenomena*, 2nd ed.; John Wiley & Sons, Inc.: New York, 2002; p xii−895.